Low-Loss III–V Semiconductor Optical Waveguides

Robert J. Deri, *Member, IEEE*, and Eli Kapon, *Senior Member, IEEE*

(Invited Paper)

***Abstract*—We review recent progress in low-loss III–V semiconductor integrated optics for the 1–1.6 μm wavelength range, including propagation, bending, coupling, and modulator losses. Tradeoffs between loss and other performance issues are discussed in detail.**

I. Introduction

Semiconductor waveguides are the "wires" used to route optical signals on a semiconductor chip, which provide the basis for numerous integrated optic devices (e.g., power dividers, filters, switches, and modulators) suitable for applications such as lightwave telecommunications, optical signal processing, and sensors. It has long been recognized that III–V semiconductors offer significant advantages over other materials such as $LiNbO_3$ or glass for many applications [1]. These include: 1) the potential for monolithic integration with other optoelectronic (e.g., lasers, detectors) and electronic (transistor) devices to enhance the functionality of transmitter and receiver circuits using additional guided-wave signal processing; 2) suitability for high-speed low-drive voltage modulators and switches [1], [2], with further advances expected from multiple quantum well (MQW) technology [3]; and 3) the availability of sophisticated, controllable fabrication processes (e.g., epitaxial growth, selective etching) and simple methods for endfacet preparation (scribe-and-cleave versus cut-and-polish). For these reasons, interest in III–V semiconductor guided-wave devices continues to grow, particularly as single-mode optical fiber is increasingly accepted for communications transmission applications.

The advantages offered by III–V materials, however, have historically been offset by the high insertion loss (>3 dB) of semiconductor waveguide devices and the large size (≥ 1 cm) of conventional integrated optic circuits. Device insertion loss directly reduces the maximum transmission length of communication systems, and is therefore highly undesirable. While laser gain in III–V materials offers the potential to offset such insertion loss, this approach to loss reduction is frequently undesirable due to the additional amplification noise and greater complexity in both integrations and systems use. A second issue is large device size and incompatibility with the relatively high cost of III–V semiconductor materials, which places a premium on compact device design [4]. Nonetheless, significant progress has occurred in the areas of loss and chip size during the past several years.

This paper reviews these recent advances in low-loss, compact III–V semiconductor waveguide technology for the λ = 1–1.6 μm (fiber telecommunications) wavelength range, with emphasis on the impact of improved fabrication on insertion loss, device size versus loss tradeoffs, and the use of epilayer design for loss reduction. Mechanisms of waveguide loss are first discussed in detail, followed by a short review of loss measurement techniques. We then review the performance achieved with low-loss passive structures (straight and bent guides), and the additional constraints on realizing low-loss active devices (modulators, switches) from passive waveguide circuits. Finally, we discuss areas of current research interest, and conclude with prospects for future guided-wave applications of III–V semiconductors.

Manuscript received June 22, 1990; revised December 20, 1990.
The authors are with Bellcore, Red Bank, NJ 07701.

II. Waveguide Loss Mechanisms in III–V Materials

Fig. 1 shows a schematic of a typical semiconductor waveguide structure, as realized on a GaAs substrate. Optical confinement (waveguiding) is achieved in the vertical direction perpendicular to the substrate plane by refractive index differences due to material compositional changes, and in the lateral direction by "effective index differences" [5] due to a rib etched into the material layers. Epitaxial growth is usually employed to obtain the required material. The most common methods for achieving lateral optical confinement employ a rib geometry, etched either after layer growth as in Fig. 1, prior to growth to achieve a "buried rib" geometry, or between two growth steps to achieve a buried-heterostructure geometry (regrowth over rectangular guide layer [6]. Other methods of lateral confinement include the use of index caused by material strain (photoelastic effect) [7], carrier in-diffusion [8], or superlattice disordering [9]. Loss sources in such waveguides can be classed as either absorption, scattering, or leakage. Absorption arises from imperfect material transparency, while scattering and leakage involve the transfer of optical energy from guided waves to nonguided radiation. Scattering arises from imperfect refractive index distributions (e.g., interface roughness), whereas leakage can occur even for ideally smooth structures. The exponential attenuation of optical power in the guided mode is described by the loss (extinction) coefficient α.

A. Absorption

Many III–V semiconductor alloys exhibit a direct bandgap, and absorb strongly at wavelengths shorter than the corresponding band edge. In practice, such absorption is readily avoided by appropriate choice of alloy composition and operating wavelength. In some applications, however, such as electroabsorption modulators (e.g., [2]), residual band edge absorption can play an important role. In applications involving monolithic integration of transparent waveguides with lasers or detectors, which require material with bandgaps below the photon energy, the guided wave must be confined to regions of reduced absorption to minimize losses. This can be accomplished by a number of techniques, including selective removal of absorbing material [11], bandgap changes due to disordering of quantum well material [9], [10], or growth of patterned quantum wells on nonplanar substrates [12].

0018-9197/91/0300-0626$01.00 © 1991 IEEE

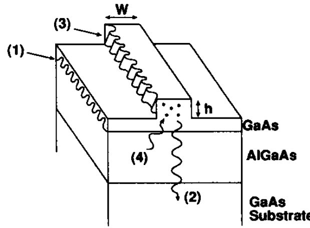

Fig. 1. Schematic GaAs-AlGaAs rib waveguide, with loss mechanisms indicated: (1) epilayer roughness, (2) substrate leakage, (3) rib sidewall roughness, and (4) defect and impurity absorption. Rib width W and height h are shown.

Absorption is also introduced by free carriers, and the initial achievement of high-transparency GaAs waveguide material was primarily due to reduction of residual carrier concentration [13], [14]. In general, free carrier absorption involves both intra- and interband transitions, and thus cannot be predicted from a simple Drude conductivity model. While the Drude model provides a correct conceptual description of intraband absorption, the Drude damping time is wavelength-dependent and cannot be determined from dc measurements (e.g., Hall mobility). Typical bulk losses for n-type material ($1 \times 10^{18}/\mathrm{cm}^3$) are 22 and 4 dB/cm for GaAs and InP at $\lambda = 1.5$ μm, respectively, [15]-[17]. The greater valence band complexity causes significantly higher absorption in p-type III-V materials [17]-[21], typically 56 dB/cm for both GaAs- and InP-based alloys with $p = 10^{18}/\mathrm{cm}^3$ at $\lambda = 1.3$ μm [21]. This high p-type material absorption is quite important for a variety of guided-wave devices requiring p-n junctions, such as carrier injection and depletion modulators and semiconductor lasers. The absorption loss of a given waveguide mode depends both on bulk material losses and the overlap of the modal intensity distribution with the absorbing material. In applications where absorbing material must be employed, as for electrodes in electrooptic devices, waveguide absorption can be reduced by minimizing this overlap "fill factor" (see Section IV).

The presence of deep (near-midgap) energy levels also introduces material absorption. Deep levels can be incorporated during crystal growth; typical bulk losses for the deep defects responsible for semiinsulating behavior are 3.5 and 1 dB/cm in GaAs (EL2 level) [22] and InP (Fe doping) [23], respectively, for $1 \times 10^{17}/\mathrm{cm}^3$ concentration at $\lambda = 1.5$ μm. Significant deep level absorption has been suggested for waveguides grown on semiinsulating substrates [24]; these losses may limit waveguide performance in optoelectronic integration applications for which semiinsulating material is required. Dislocations may introduce deep level absorption as well; an extreme example is the high dislocation density resulting from lattice-mismatched crystal growth of GaAs guiding layers on InP, for which defect absorption ≥ 9 dB/cm can occur [25]. Finally, waveguide processing can also generate absorbing layers: examples are proton bombardment, as employed in early III-V waveguide fabrication [26]; and ion milling, which introduces sputtering damage [27] when used for rib etching.

B. Scattering

Scattering loss in state-of-the-art III-V waveguides results primarily from rough interfaces (both epilayer boundaries and etched rib surfaces) rather than volume inhomogeneities. Attempts to quantitatively predict scattering losses from *a priori* theories and measured roughness values are complicated by the two-dimensional nature of channel waveguide transverse index distributions, the dependence on both the amplitude and *spatial periodicity* of the roughness, and the difficulty in measuring small amplitude/periodicity aspect ratios. Theoretical treatments are available for scattering in *planar waveguides* (with no channel definition and thus only one-dimensional optical confinement) [28]-[30], which are probably adequate for estimating epilayer scattering loss in channel guides with weak lateral optical confinement. First-order scattering of light at wavelength λ is expected from roughness of spatial period Λ in the range

$$\lambda/(n_1 - n_2) > \Lambda > \lambda/(n_1 + n_2) \tag{1}$$

where n_1 and n_2 are waveguide core and cladding indexes [29]. Periodicities from several hundred microns down to several tenths of a micron can thus contribute to scattering. This roughness distribution is difficult to access experimentally over the wide range of spatial periodicity, particularly for small roughness amplitude. For these reasons, the easiest models to employ for comparison to experiment are those requiring only the roughness amplitude; however, additional (possibly unwarranted) assumptions about the periodicity distribution must be employed. One such model, proposed by Tien [31], predicts 0.5 dB/cm scattering loss at 1.5 μm wavelength for only 4 nm of epilayer roughness in a typical waveguide structure (1.5 μm thick core GaAs-AlGaAs single heterostructure). We again stress that microscopic observation of such small amplitudes is complicated by the large (100 μm) periodicities which must be considered.

Tien's formula [31] for the scattering loss α of symmetric planar guides can be written as

$$\alpha = \frac{4\sigma^2 h^3}{\beta(t + 2/p)} = \frac{\sigma^2 k_0^2 h}{\beta} \frac{E_S^2 \Delta n^2}{\int E^2\, dx} \tag{2}$$

where σ is the interface roughness, t is the guide thickness, k_0 is the free-space wavenumber, β is the modal propagation constant, Δn^2 is the difference in dielectric constants (indexes squared) between the guiding and cladding layers, and where h, p are transverse propagation constants in the guide, cladding, respectively. Equation (2) also shows that the scattering is explicitly proportional to the normalized optical intensity at the guide-cladding interface $E_S^2/\int E^2\, dx$. In general, epilayer scattering increases with increasing index difference $\Delta n = n_1 - n_2$, decreasing guiding (core) layer thickness, increasing mode number, and σ^2. Numerical evaluation of (2) suggests that α scales approximately as t^{-3} for sufficiently thick structures with fixed Δn and as $(\Delta n)^2$ for single-mode guides.

Models for scattering from rib sidewall roughness ideally require a full two-dimensional (2-D) treatment of the waveguide cross section, adding additional complexity. Recent theoretical developments have led to quantitative sidewall scattering predictions based on finite element, 2-D modal simulations, including the dependence of the roughness periodicity [32], [33]. A simple alternative, which avoids the full 2-D modal solution, employs an "effective index approximation" [5] to describe the rib as an equivalent 1-D transverse index distribution, which is then treated identically to the epilayer scattering problem discussed above. In this approach, which implicitly assumes that guided light is scattered into planar waveguide modes outside the guiding channel, Tien's model [31] suggests that sidewall scattering loss in single-mode guides increases with the square

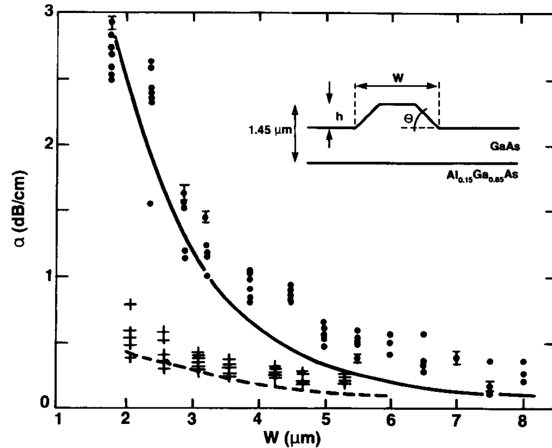

Fig. 2. Straight guide propagation loss versus rib width for structures exhibiting rib sidewall scattering at λ = 1.52 μm [34]. Upper experimental data (points) pertain to guides with deep rib etch (h = 0.35 μm); lower data (crosses) pertain to guides fabricated from the same epilayers with shallow rib etch (h = 0.12 μm). Curves correspond to calculations based on the effective index approximation and 50 nm rms sidewall roughness. Epilayer structure is inset.

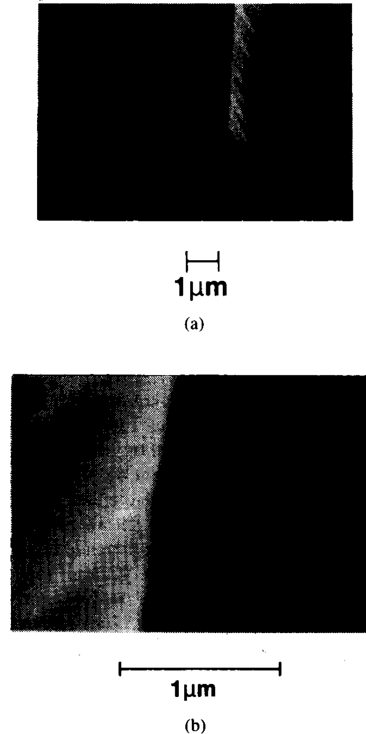

Fig. 3. Scanning electrons micrograph of a wet-chemically etched GaAs-AlGaAs waveguide rib, showing typical sidewall roughness [14]: (a) perspective view of rib; (b) magnified top view of rib.

of the roughness amplitude, the square of the effective index difference Δn_{eff} describing the optical confinement provided by the waveguide rib, and with decreasing rib width. Fig. 2 shows experimental results for guides with large sidewall scattering losses. Experimental observations typically indicate rib sidewall roughness amplitudes in the 10–100 nm range [13], [14], [34]–[36], as shown in Fig. 3. For this roughness magnitude, Tien's model predicts significant sidewall scattering (>1 dB/cm) for single-mode guides with Δn_{eff} exceeding 10^{-2}. A key prediction of such effective index modeling is that sidewall scattering depends only on rib width and Δn_{eff}, and is independent of other structural details (e.g., single- or double-heterostructure) provided that Δn_{eff} is fixed. The qualitative dependence of scattering on guide structure, as determined from finite difference simulations of the full two-dimensional waveguide mode [37], suggests that single- versus double-heterostructure differences do not in fact significantly affect sidewall scattering. This conclusion is further supported by GaAs–AlGaAs waveguide experiments showing nearly identical loss for both structures [14], [34] even at large $\Delta n_{eff} = 10^{-2}$ [38].

Theoretical predictions for waveguide loss can be extremely useful for the development of low-loss waveguide technology by suggesting experimental methods for distinguishing between different loss mechanisms. For example, the λ dependence of the propagation loss α can be used to distinguish between scattering and absorption (if bulk absorption $\alpha(\lambda)$ is known), the temperature dependence can distinguish free carrier effects (cooling to remove carriers from the conduction band), and the epilayer structure dependence can be used to distinguish absorption overlap and epilayer scattering effects. Such experiments are relatively difficult to perform, however, and the most common diagnostic is dependence on rib width W and rib etch depth h [14], [34], [39], [40], as in Fig. 2. For structures operated far from the fundamental mode cutoff, observation of W-dependent α indicates that loss results from imperfections induced during rib fabrication. Finite difference simulations have shown that similar W dependence results from both imperfections localized on the rib sidewall and those uniformly distributed over the etched surface [37]. Thus, W dependence may reflect rough sidewalls (poor lithography), rough etching, or absorption in etched surfaces (dry etching damage), and cannot be used to discriminate between these different loss mechanisms. Imperfections localized on the rib sidewalls can be distinguished from those uniformly distribued over the etched area (geometries shown in Fig. 4) by the $\alpha(h)$ dependence; simulations show that sidewall imperfections exhibit a strong $\alpha(h)$ dependence (e.g., due to changes in Δn_{eff} with h), whereas uniform etch imperfections do not (Fig. 4) [37]. Therefore, the $\alpha(h)$ dependence provides a more complete diagnostic of fabrication-induced losses than is obtainable from $\alpha(W)$ alone.

The absorption and scattering losses discussed above are assumed to be evenly distributed over length scales which are short compared to typical devices, and can be described by a propagation loss coefficient α in dB/cm. Additional loss can result from discrete imperfections of low density, in which case guide insertion loss is not simply proportional to guide length. Such defects have been detected from the length dependence of insertion loss in InP guides [41], and can be described statistically under the assumption of random spatial distribution. Statistical parameters deduced for the InP-based waveguides of [41], which were fabricated using conventional growth and processing techniques, are a probability of 1.5 defects/cm and average loss ≈ 0.1 dB/defect far from cutoff [41]. Discrete defect loss increases significantly for operation close to the cutoff condition of the guided mode due to the weaker optical confinement. Fig.

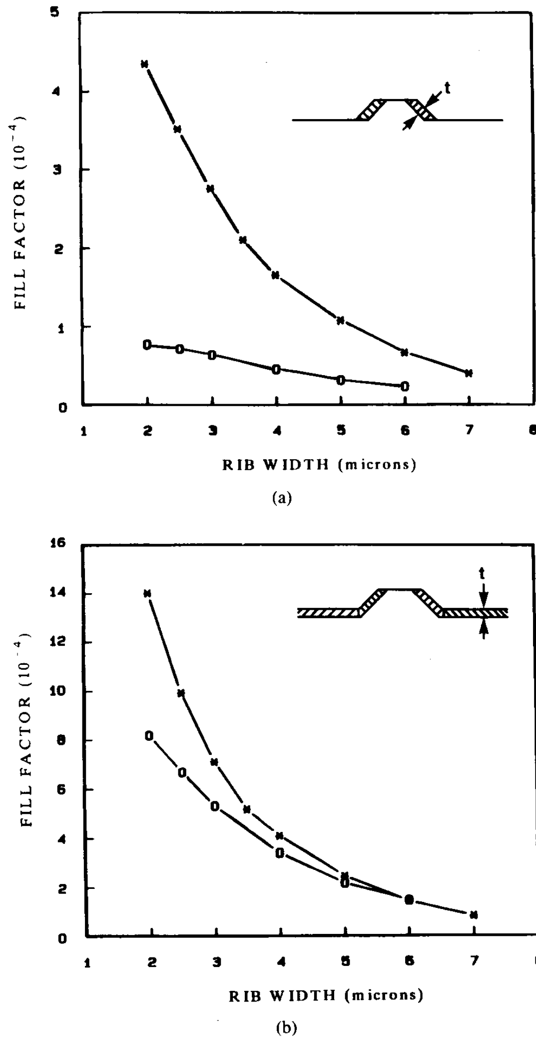

Fig. 4. Finite element simulation of the dependence of scattering loss on rib width W and etch depth h for the structures of Fig. 2, with rib angle $\Theta = 45°$ and damage depth 50 nm [37]: (a) dependence of relative scattering loss on W and h for sidewall damage or roughness, localized to damaged area t shown by shaded area of rib in inset; and (b) dependence of relative scattering loss on W and h for uniform damage or roughness, with damaged area t shown by shaded area of rib in inset.

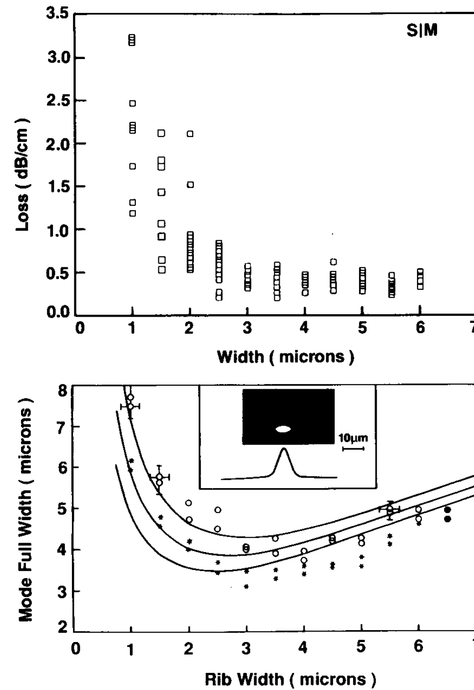

Fig. 5. Effect of discrete defects: correlation of propagation loss and lateral mode size (full width at half maximum intensity) as a function of rib width for InGaAs-InP multiple-quantum-well waveguides [41]. Each loss datum was obtained for a separate waveguide of length 9.4 mm at $\lambda = 1.52$ μm. Inset shows a photograph of the near-field distribution for a rib width of 5.5 μm.

5 shows the W dependence of both α and the lateral waveguide mode size; as W decreases below 3 μm, the mode size increases (due to weak confinement), and both the magnitude and spread of measured α values increase as expected for discrete defect losses. Notably, discrete defects cause significant spread in α among nominally identical guides, even far from cutoff ($W >$ 3 μm). While such discrete defects have received little attention in the literature, their practical importance is generally recognized: they complicate propagation loss measurements and interfere with proper operation of guided-wave devices requiring equal losses in different optical paths (e.g., Mach–Zehnder interferometers and 3 dB couplers for balanced coherent reception).

C. Leakage

Waveguide losses can also result from radiation losses in the absence of scattering from interfaces. When the waveguide is supported on a substrate of equal or greater refractive index, leakage of guided light into the substrate occurs. This situation exists for the GaAs–AlGaAs material system (Fig. 1), for which thick AlGaAs cladding layers are required to minimize leakage loss [1], [14], [42]. For Al mole fractions $<10\%$, cladding thickness >4 μm is required to maintain leakage loss below 0.1 dB/cm [14]. In general, the loss coefficient due to leakage decreases exponentially with increasing cladding thickness T. For the GaAs–AlGaAs single-heterostructure of Fig. 1, the leakage-induced propagation loss of the fundamental TE mode is given by

$$\alpha \approx \lambda^3 hp^2 \sin^2 (ht) \exp(-2pT)/\pi^3 n \Delta n^2 t \qquad (3)$$

where λ is the free-space wavelength, n and t are the GaAs guiding layer index and thickness, Δn^2 is the difference in the squares of the indexes between the GaAs guiding and AlGaAs cladding layers, h and p are transverse propagation constants in the GaAs and AlGaAs, and T is the AlGaAs cladding thickness [1]. Equation (3) is derived for planar waveguides, and should be applicable to channel guides with weak lateral optical confinement.

When waveguides are bent in a continuous fashion (e.g., circular or S-bends), some guided light is lost to radiation; this distributed radiation loss (measured in dB/cm or dB/degree) is analogous to leakage [43]–[45]. The analogy to leakage can

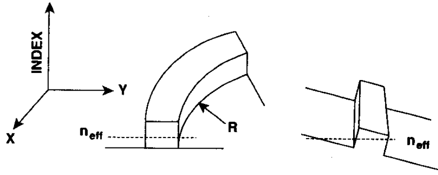

Fig. 6. Change in refractive index distribution obtained by conformal mapping a bent guide into an "effective straight guide." Leakage occurs into region of the mapped structure outside the rib for which $n_{mapped} > n_{eff}$ [44].

be qualitatively understood using conformal mapping techniques, which describe bent planar guides by corresponding straight, *leaky* guides with the transverse index distribution shown in Fig. 6 [44], [45]. Theoretical models are available for distributed loss in 1-D cross-sectional planar guides [43], [44], and can be used to model rib waveguide bends using effective index methods. This approach reasonably describes the experimental behavior of structures in which the etched region outside the semiconductor rib supports a planar waveguide mode [46], although more sophisticated modeling can achieve somewhat better accuracy (Fig. 7) [47], [48]. Distributed bend loss increases with radius R in a nearly exponential fashion, as shown in Fig. 7. This behavior is consistent with the exponential behavior predicted for bend loss in planar (slab) guides [43], [44]

$$\alpha = K \exp(-cR), \qquad \text{where } c \approx \beta(2\Delta n_{eff}/n_{eff})^{3/2} \qquad (4)$$

where K is a constant depending on the guide thickness and indexes, $\beta = 2\pi n_{eff}/\lambda$ is the modal propagation constant, and Δn_{eff} is the difference between the modal effective index and the cladding index. Equation (4) assumes $\Delta n_{eff}/n_{eff}$ is small and that the bending is a small perturbation on the modal intensity distribution of the straight guide mode. The exponential behavior means the loss increases abruptly for radii below some critical value. Fig. 8 shows the dependence of this critical radius R_1, defined as the point where bend loss is 1 dB/90°, on the rib etch depth h (i.e., variable Δ_{eff}). For small etch depth, and hence small Δn_{eff}, R_1 varies as $\Delta n_{eff}^{-3/2}$ as predicted by (4) [43], so that a tradeoff exists between small bend size and increased scattering loss ($\alpha \propto \Delta n_{eff}^2$).

For sufficiently deep rib etch depth h, the region outside the rib does not support planar waveguide modes, and the effective index approach used above is not applicable. Because such deeply etched ribs provide the most compact bend performance, bend loss computation for these structures has recently received much attention, using a variety of sophisticated simulation methods [49]–[51]. These computations predict a rapid, near-exponential rise in bend loss with decreasing radius, just as for guides with shallowly etched ribs discussed above. Because distributed bend radiation loss increases with decreasing radius R, while propagation loss in the bend due to absorption and scattering increases proportionally to R, there will be an optimum R value which minimizes the total bend loss.

Modal mismatch (nonadiabatic changes in guided-mode transverse field distributions) can also cause radiation loss from discrete transitions in semiconductor waveguide circuits. Examples are the junctions between straight and continually curved guides [43], curvature reversal in S-bends, abrupt waveguide bends [52], [53], tilt misalignment in integrated mirrors [54], and coupling from the III–V guides to external optical fibers [55]. Modal mismatch loss can be calculated from modal field overlap integrals, which include phase variations to account for

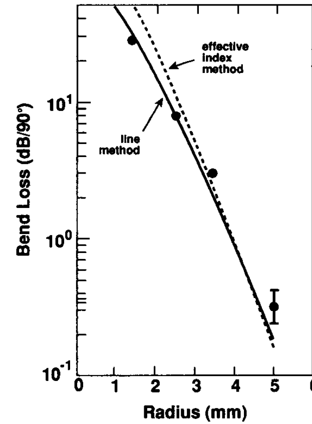

Fig. 7. Dependence of circular bend loss on radius for the structure of Fig. 2 (inset, $W = 3$ μm, $h = 0.33$ μm) [47]. Results of experiment [46], simple effective index model [46], and more accurate theory [47] are shown.

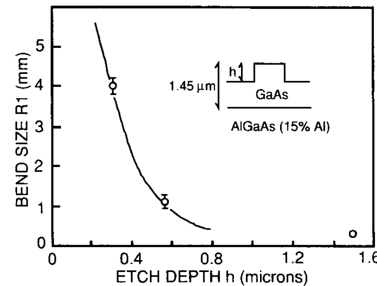

Fig. 8. Dependence of critical bend radius for low loss R_1 on rib etch depth h for the structure of Fig. 2 (inset). Solid points show experimental data of [46] and [91], and solid curve shows calculated behavior based on an effective index approximation and theory of [43].

tilt or bending effects [54], [55]. Thus, this loss mechanism is readily calculated in single-mode structures, provided that the correct 2-D transverse modal fields are known. In the case of continuous bends connected to straight guide sections, both mismatch and distributed radiation contribute to bend insertion loss; planar guide calculations suggest that mismatch effects dominate the loss at wider guide width [43]. Fig. 9 shows the calculated modal intensity distribution for light in a bent rib guide; significant deviations from symmetry about the rib center indicate bend-induced mode distortion which results in mismatch loss [47]. Such bend-induced changes have been experimentally observed in bent rib waveguide near-field patterns [56]. Mismatch also plays a critical role in coupling from semiconductor guides to other on-chip optoelectronic devices.

D. Polarization Dependence

Finally, it should be noted that optical waveguide losses may depend on the state of polarization of the guided light. This may result simply from differences in the optical intensity distribution between different polarizations, causing different overlap with scattering and absorptive material regions. As an extreme example, polarization-dependent boundary conditions can be utilized to create waveguide polarizers in which one polariza-

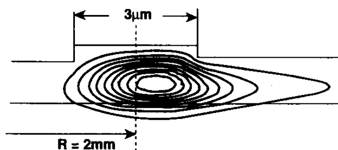

Fig. 9. Modal intensity distribution in a circularly bent waveguide with the structure of Fig. 2 (h = 0.33 μm) and 2 mm radius [47].

tion is much more strongly absorbed by a metal film overlaying the guide; such polarizers can be significantly altered by insertion of low-index insulating layers between the guiding and metallic regions [57]. Polarization also can affect waveguide leakage losses. One example is the strong dependence of bend radiation loss on polarization [48] due to the polarization-dependence of Δn_{eff}; another is polarization-dependent cutoff conditions for the fundamental guided mode due to birefringence in superlattice waveguides [58], [59], which can cause large leakage of TM modes in these structures.

III. Waveguide Loss Measurements

The simplest method for evaluating waveguide insertion losses is measurement of their attenuation using transmission experiments. The ratio of output to input optical intensities yields the overall insertion loss, which includes both coupling and on-chip losses. The standard approach used to distinguish coupling and propagation losses in straight waveguide samples has been to measure the loss as a function of guide length (the "cutback method"), which is varied by sequential cleaving [40]. The major difficulty with this technique is input coupling reproducibility, which is typically ±0.1-0.2 dB for guides mode matched to single-mode fiber [24], [60], [61], however, typical semiconductor guides exhibit smaller mode sizes which result in more severe alignment tolerances. Coupling reproducibility thus limits the overall accuracy of this measurement, particularly when sample length is varied to separate the effects of propagation and coupling losses. A second difficulty is caused by waveguide endfacet reflections, which give rise to resonator effects that significantly complicate data analysis. Resonator attenuation does not vary linearly with guide length [62], and back-reflected light can cause feedback effects if the measurement light source is not properly isolated [63]. Such resonator effects can be avoided by antireflection coating the endfacets [24] or by using incoherent light (e.g., LED source) for the measurement.

An important variant of such transmission methods permits extraction of both coupling and on-chip losses from data obtained with samples of fixed length. If input cooling is achieved using well-characterized methods (e.g., single-mode fiber butt coupling), on-chip and coupling losses can be distinguished from two measurements on the same structure: one with identical single-mode output coupling and one which collects all the output light (lens or multimode fiber) [24], [64]. This method assumes identical input and output single-mode coupling, and thus is limited by coupling reproducibility. It is also assumed that no stray light is collected by the output lens. An alternative variant employs only a single loss measurement, using measured modal intensity distributions to calculate the coupling losses [60], [61]; negligible coupling misalignment loss is assumed.

In order to circumvent problems with input coupling reproducibility, on-chip losses can be measured using Fabry-Perot

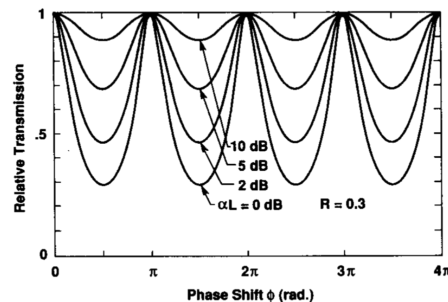

Fig. 10. Simulated Fabry-Perot fringes (transmission versus phase) for facet reflectivity of 0.3 and on-chip losses of 0, 2, 5, and 10 dB, as indicated.

contrast methods [62], [65], [66]. This technique relies on cleaved waveguide endfacets to form a Fabry-Perot waveguide resonator, the finesse of which is measured by varying the waveguide phase ϕ using thermal [62], [65], [66], wavelength [67], or electrooptic modulation tuning [68]. The transmission T of such a waveguide resonator, consisting of a straight waveguide of uniform propagation loss α and length L is given by

$$T(\phi) = (1 - R)^2 e^{-\alpha L}/[(1 - r)^2 + 4r \sin^2 \phi] \tag{5}$$

where R is the endfacet reflectivity, $r = Re^{-\alpha L}$, and ϕ is the phase which is varied during the measurement. Fig. 10 shows simulated Fabry-Perot fringes for several values of αL and a typical semiconductor cleaved facet reflectivity (R = 0.3). Measurement of the fringe contrast K given by

$$K = (T_{max} - T_{min})/(T_{max} + T_{min}) = 2r/(1 + r^2) \tag{6}$$

yields r uniquely. Notably, (6) shows no dependence on the input coupling, and thus coupling reproducibility problems are avoided. The simplest application of this technique relies on a single measurement of resonator contrast K at fixed length L to determine r, with αL deduced from r using an assumed facet reflectivity value R. In general, however, the waveguide reflectivity differs from the simple Fresnel value [69] so that use of simple calculations for R leads to inaccurate α results. Although models for waveguide modal reflectivity do exist [69], [70], small discrepancies between calculated and actual mirror performance can have large effects on the deduced propagation loss, particularly for $\alpha < 1$ dB/cm. An improved version of the Fabry-Perot method involves multiple measurements of K with variable sample length L [14], [71]; since

$$\ln [1 - (1 - K^2)^{1/2}/K] = \ln R - \alpha L \tag{6}$$

R and α can be independently determined from a plot of the left-hand side of (6) versus L. This procedure is illustrated in Fig. 11(a), which shows typical Fabry-Perot fringe data and results of the sequential cleaving experiment for a GaAs-AlGaAs ridge waveguide [14]. The reflectivity R deduced from such a measurement can be used to extract α from fixed-length K values measured for other guides fabricated on the same chip; typical results of such a procedure are shown in Fig. 11(b).

The major advantage of the Fabry-Perot technique is its inherent reproducibility and insensitivity to coupling misalignment, which permit more accurate measurement of small on-chip losses than transmission loss methods. In the authors' laboratory, reproducibility for a fixed waveguide sample is ±0.02 dB, and facet reflectivity reproducibility in sequential cleaving

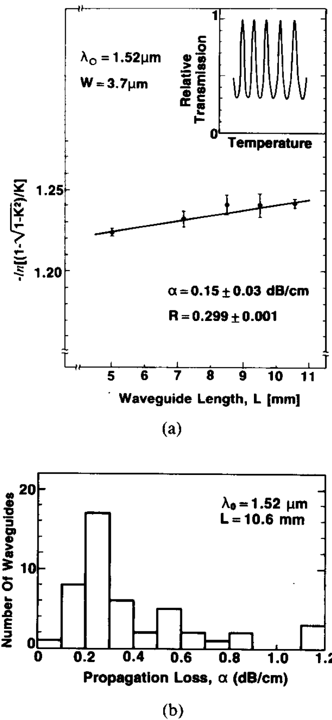

Fig. 11. (a) Typical experimental Fabry-Perot data obtained using a cutback technique to separate propagation loss and facet reflectivity [14]. Inset shows experimental fringes. (b) Histogram of losses determined for many single-mode guides on the same chip.

is ±0.05 dB. On-chip loss above ≈ 10 dB results in low fringe amplitude (see Fig. 10) and hence less accurate measurements; thus, transmission loss techniques are preferred for measurement of larger losses. On the other hand, it is difficult to distinguish on-chip loss below ≈0.1 dB because it results in small changes in fringe amplitude, which is primarily determined by the modal reflectivity. Measurement of smaller losses may require longer sample length (for straight guide α determination) or high-reflectivity endfacet coatings to increase the intrinsic resonator finesse. The major disadvantage of Fabry-Perot methods is the necessity of measurements at several sample lengths to correctly evaluate the endfacet modal reflectivity. It should also be noted that the Fabry-Perot method is not restricted to measurements of spatially uniform propagation losses in straight guides. The method can also be employed to measure spatially nonuniform losses, such as a combination of bend radiation, straight guide propagation, and bend-to-straight guide modal mismatch loss in a typical S-bend structure. In fact, the quantity αL used in the above discussion of the Fabry-Perot method actually represents $\int \alpha(x)\, dx$ along the waveguide structure.

An additional limitation of the Fabry-Perot technique is its restriction to single-mode propagation. If optical waves of different phase velocity are simultaneously excited in the waveguide under test, the resultant observed response is a superposition of the resonance fringes for each phase velocity. It can be shown that, for a static superposition of modes, the deduced loss under multimode excitation is always greater than the loss of the least lossy mode. For this reason, it is frequently stated that the Fabry-Perot method always provides an upper limit to the true loss. This conclusion is misleading, however, because it only applies to static excitation at fixed guide length. Under time-dependent modal excitation (time-dependent laser multimode spectrum or input coupling), loss underestimation is also possible. Likewise, losses deduced from sequential cleaving measurements can be skewed in either direction due to changing multimode excitation for each sample length. Therefore, proper implementation of Fabry-Perot measurements requires a single-frequency laser source and single-mode waveguides. It should also be recognized that improper coupling to *single-mode* waveguides can lead to incorrect measurement due to stray light collection (a particular problem for short guide length ≤2 mm), which effectively leads to *multimode* measurement conditions. The technique cannot in general be applied to devices employing multiple interacting guides (more than one supermode), such as Mach-Zehnder interferometers and directional couplers, in a straightforward fashion; however, accurate device losses can be determined from combined Fabry-Perot and transmission techniques [72] and/or more complex analysis [73]. For the special case of double-mode uncoupled waveguides, reasonable measurements can be obtained provided that the input coupling is carefully chosen, an aperture is used to exclude the higher-order mode from the output coupling, and minimal intermode scattering occurs [34]. Output apertures are also useful for measurements of single-mode structures to eliminate errors due to stray light collection.

To summarize, direct transmission measurements are relatively simple to perform and widely applicable, but are limited to measurement of higher losses by coupling reproducibility. Fabry-Perot methods differ greater sensitivity to small on-chip losses at the expense of more complexity, single-mode restrictions, and the inability to provide coupling loss data. The majority of III-V loss measurements have utilized one of these two techniques; however, additional methods, such as those based on out-of-plane scattering or photothermal deflection [74], [75], can also provide useful capabilities.

IV. Current Low-Loss III-V Waveguide Performance

A. Passive Guiding Structures

To realize straight waveguides with low propagation loss, high-quality epitaxial material is required to minimize epilayer scattering and absorption losses. Liquid phase epitaxy (LPE), historically one of the first useful III-V growth techniques, has generally proved less satisfactory due to epilayer roughness; typical propagation losses are ≥5 dB/cm [1], [76], with the lowest reported value of 2 dB/cm [35]. The advent of alternative growth methods, such as organo-metallic chemical vapor deposition (OMCVD) and molecular beam epitaxy (MBE), has greatly reduced this problem. By 1987, there were several reports of single-mode or quasi-single-mode waveguides with α ≤ 0.3 dB/cm using GaAs-AlGaAs epilayers [13], [14], [34], [39], [77], with many more reports in the range below 1 dB/cm as reviewed elsewhere [78]. By 1989, there were several reports of single-mode guides on InP with α ≤ 0.5 dB/cm [6,] [24], [41], [71], [79], [80], and the feasibility of obtaining a high yield of such guides over a reasonable chip area (9 × 5 mm^2) was demonstrated [41]. In general, the lowest losses have been in the range 0.1-0.2 dB/cm, and are approaching measurement limits imposed by available sample size, experimental accuracy

TABLE I
REPRESENTATIVE STRAIGHT GUIDE PROPAGATION LOSSES AT λ = 0.8–1.6 μm

Material	Growth Method[a]	λ (μm)	Structure[b]	α (dB/cm)	Reference
on GaAs					
AlGaAs–AlGaAs	OMCVD	0.83	DH, SM(?)	0.1	[77]
GaAs–AlGaAs	OMCVD	1.15	DH, SM	0.65	[39]
GaAs–AlGaAs	OMCVD	1.3	SH, MM(?)	0.2	[13]
GaAs n^-/n^+	OMCVD	1.3	SH, SM	0.8	[13]
GaAs–AlGaAs (MQW)	OMCVD	1.52	DH, SM	0.15	[14]
GaAs–AlGaAs	OMCVD	1.52	SH, SM	0.2	[34]
GaAs–AlGaAs	MBE	1.15	SH, SM	1.9	[113]
InGaAs–GaAs	MBE	1.15	SH, SM	0.6	[114]
GaAs–AlGaAs (MQW)	MBE	1.3	IID-BH, MM	1.8	[9]
GaAs–AlGaAs	MBE	1.52	DH, SM	0.4	[68]
GaAs n^-/n^+	VPE	1.06	LE, SM(?)	1.5	[115]
GaAs n^-/n^+	LPE	1.3	SH, SM	2	[35]
on InP					
InGaAsP–InP	OMCVD	1.52	DH, SM	0.18	[80]
InGaAsP–InP	OMCVD	1.52	BH, SM	0.18	[6]
InGaAs–InP (MQW)	OMCVD	1.52	DH, SM	0.24	[41]
InGaP–InP	OMCVD	1.32	DH, MM	1.25	[116]
InGaAsP–InP	CBE	1.67	ARROW	0.9	[100]
InAlAs–InP	MBE	1.15	SH, SM	4	[117]
InGaAlAs–InAlAs	MBE	1.3	DH, SM	3.4	[118]
InGaAlAs–InP	MBE	1.55	SH, MM	2.2	[119]
InGaAsP–InP	LPE	1.3	BH, SM	6	[76]
Lattice-mismatched					
GaAs–AlGaAs on Si	OMCVD	1.3	SH, SM	0.95	[81]
GaAs–AlGaAs on InP	OMCVD	1.52	SH, SM	0.9	[82]

[a]CBE = chemical beam epitaxy, VPE = chloride beam epitaxy, other symbols defined in the text.
[b]SH (DH) = single (double) heterostructure, BH = buried heterostructure, IID = impurity-induced disordered, SM (MM) = single (multi)mode.

(typical uncertainties are ±0.05 dB/cm [6], [14], [24], [34], [39], [71]), and extraneous loss contributions from discrete defects [41]. The use of superlattice or MQW material in guiding [24], [41] or cladding [14] layers has been shown to be compatible with low-loss performance, despite the large number of interfaces in such structures. These results indicate that few midgap absorbing defects are generated at the interfaces; the low α achieved, even at large MQW periodicities comparable to a quarter optical wavelength [24], show the feasibility of extremely smooth layer interfaces with low scattering loss. These results show that the realization of straight waveguides with low α on GaAs and InP is now well established for GaAs- and InP-based material. Table I surveys some of the lowest-loss straight channel guides obtained using a variety of different III-V materials, crystal growth techniques, and wavelengths; this table is intended to show representative results for a wide variety of materials and structures, and does not provide an all-inclusive survey. Even highly lattice-mismatched materials (e.g., GaAs on Si or InP), where material quality is degraded, have yielded guides with α below $\approx$1 dB/cm using sufficiently thick buffer layers to isolate the guiding region from the mismatched interface [81], [82].

Many of the reported low-loss single-mode guides exhibit the same basic structure. In general, a thick guiding layer (1–3 μm) and small guide-cladding layer index difference (2–10 × 10^{-2}) are used to minimize scattering from epilayer roughness [14], [34], [39], [41], [78]; smaller index difference is less frequently employed due to increasing difficulties with the control of smaller changes in alloy composition. It may be possible to reduce epilayer scattering by compositionally grading the heterointerfaces [39] or by using superlattices to reduce surface roughness [14], [77], [83]. Small rib $\Delta n_{eff} << 10^{-2}$ is chosen to minimize fabrication-induced rib scattering loss, using wide ribs (4–8 μm) to operate with well-confined modes and reduce scattering from discrete defects. Under these conditions, the detailed guide structure appears to be less critical, as discussed in Section II in relation to effective index models for sidewall scattering. Comparable α is achieved for both single [13], [34], [38] and double heterostructures [14], [38], [39], [41], [71] with top-cladding ribs as well as regrown buried heterostructures [6]. Of course, operation within these limits is not essential for low-loss performance; it simply results in structures which are less sensitive to fabrication imperfections.

It can thus be seen that low propagation loss is readily achieved using well-established technology, particularly if guides are designed within certain structural constraints. Low propagation loss alone, however, is frequently insufficient for a viable integrated optics technology. Waveguide devices utilizing multiple input/output ports require bends to separate interacting waveguides; total chip size is generally determined by bend requirements, as demonstrated, for example, in recently reported Mach-Zehnder wavelength demultiplexers [38], [72]. Therefore, realization of low-loss compact bend structures is a key issue. The two most common bend geometries are integrated mirrors based on total internal reflection (Fig. 12) and continuous waveguide bends. In both cases, total insertion loss can be reduced using multimode straight guides for the bend input/output sections; single-mode structures are preferred for the majority of integrated optic device applications, however, and our discussion will be restricted to such cases.

Integrated mirrors [54], [84] are the most compact bending structures, and are also advantageous because the choice of

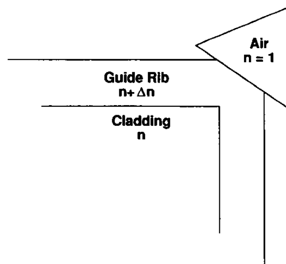

Fig. 12. Schematic of integrated mirror utilizing total internal reflection.

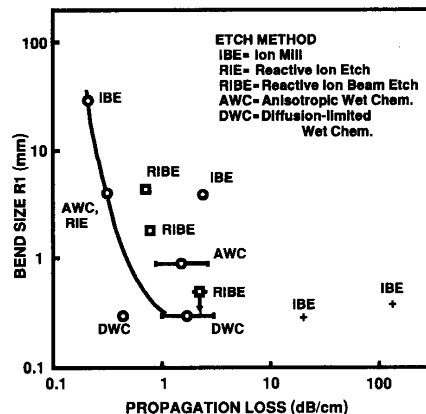

Fig. 13. Experimental results showing the tradeoff between bend size R_1 and propagation loss α for different rib etch methods in GaAs–AlGaAs rib guides [92], [93]. Circles represent data obtained with the structure of Fig. 2 (inset) at $\lambda = 1.52$ μm; boxes represent [67] and [90] at 1.5 μm; crosses represent [36] and [89] at $\lambda = 1.15$ μm.

guide structure (e.g., Δn_{eff}) is, in principle, independent of mirror design constraints. It should also be possible to realize a variety of other optical components, such as integrated beamsplitters [85], [86], with a high-performance mirror technology. At present, mirror losses are typically limited by modal mismatch to ≥ 1 dB/90° mirror, with the best results being 0.4 dB/90° mirror. Laterally self-aligned processing does not appear to reduce this loss, suggesting that the loss arises from rough surfaces and vertical tilt [84]. When mirror loss is limited by vertical tilt, the loss becomes dependent on guide structure, with better performance for smaller vertical mode size. At current loss level mirrors are less suitable for applications requiring multiple directional changes, but they remain a subject of continuing research due to their potential for extremely compact, low-loss performance. Use of mirrors to bring multiple guides into an interacting region, such as a directional coupler, involves an abrupt spatial change in guide coupling from non- to fully interacting. Such abrupt changes can prove disadvantageous because they increase crosstalk in short couplers [87]; the near-adiabatic transition obtained using continuous bends can improve device crosstalk significantly [88].

Continuous and abrupt waveguide bends are less compact than integrated mirrors, but offer the advantages of adiabatic transitions into interaction regions, a single rib etch depth (no alignment or tilt fabrication problems), and lower losses in several applications. Losses in these structures consist of modal mismatch at the straight-to-bent transitions, as well as distributed radiation and propagation loss in continuous bends. As discussed in Section II, *a tradeoff exists between bend size and propagation loss in continuous bends.* A similar tradeoff exists for modal mismatch at transitions from straight guides to continuous bends or tilted straight guides in abrupt bends, in that bend loss is reduced for smaller lateral mode size (high Δn_{eff}, small rib width). In order to achieve compact bends (large Δn_{eff}) with low guide propagation loss, smooth rib sidewalls are essential to minimize scattering. Much effort has recently focused on improved rib fabrication to achieve the necessary smooth etched surfaces [34], [36], [46], [48], [67], [89]–[93]. Fig. 13 shows the tradeoff in circular GaAs–AlGaAs waveguide bends between propagation loss and the critical bend size R_1 for which excess bend loss, excluding propagation loss, equals 1 dB/90°. Guides with smaller R_1 have more deeply etched ribs, and tend to exhibit higher α. In particular, it appears that rib etching methods involving a purely physical sputtering mechanism (e.g., ion milling) result in the largest α at fixed R_1, with lower loss achieved using etch methods based on chemical reactivity (e.g., reactive ion etching, wet chemical etching). This suggests that chemical etching techniques are the method of choice for achieving low propagation loss. Fig. 13 shows that, as R_1 is reduced over two orders of magnitude by deeper rib etching, the loss α of wet chemically etched guides increases by as little as a factor of four; the bend size–propagation loss tradeoff is almost eliminated by proper choice of rib fabrication technique. Notably, the anisotropy associated with wet etching of III–V compounds introduces no additional bend loss for radii above ≈ 900 μm in 90° bends, and poses no problem for even smaller radii in S-bend applications [93].

Using this technology, it is possible to fabricate waveguide bends with useable radii R_1 of 1–3 mm, using single-mode guides with $\alpha < 1$ dB/cm [46], [67], [90]. These guides can be used for conventional directional couplers because the region outside the rib supports a planar waveguide mode; optical confinement under the rib is relatively weak, and finite-gap coupling structures can be obtained with reasonable lengths (several mm) and gap widths accessible using conventional optical lithography (≥ 1 μm) as in [38], [72]. The corresponding total loss of such continuous bends (propagation plus bend contributions) can be as low as 0.6 dB/90° [46], which is somewhat better than current integrated mirror performance. Continuous bends offer even greater loss reductions over 90° mirrors in S-bend applications because the total bend angle is much less than 90°; for example, 1.4 mm long S-bends with 125 μm guide displacement require only 20° of circular bend, corresponding to ≈ 0.2 dB total loss.

The most compact circular bend performance is achieved using large lateral refractive index differences and structures which do not support planar waveguide modes outside the waveguide rib. Such guides can be realized using deeply etched ribs, as first suggested by Austin [36], [89]. Using such structures, bend radii R_1 as small as 300 μm can be obtained [36], [51], [89]–[91], [93]. Although scattering in these guides presents a potentially severe problem, propagation losses of 1–2 dB/cm have been achieved using etch methods suitable for smooth rib sidewalls [90]–[92]. The use of diffusion-limited wet chemical etching for rib fabrication is especially attractive, since the etchant exhibits a polishing effect which reduces the transfer of residual etch mask roughness to the rib itself [91], [92]. Using such etching, deeply etched single-mode guides with propagation loss as low as 0.8 dB/cm have been fabricated [92]. Thus,

as discussed above, the use of appropriate etching technique practically eliminates the tradeoff between bend radius and propagation loss. An alternative to deeply etched ribs, which provides comparable bend performance, is the use of buried heterostructure guides; this approach has been demonstrated on InP with low-loss bends of 300 μm radius and 3 dB/cm straight guide propagation loss [94].

A major disadvantage of continuous bends is their limitation on waveguide design parameters. In particular, bends of radii <3 mm require guide widths <3 μm for single-mode behavior (because of the large Δn_{eff} required for low bend loss), and radii <1 mm require deeply etched ribs which are incompatible with conventional directional couplers because exceedingly small gaps are required for efficient coupling. The small guide size increases the difficulty of input coupling onto the semiconductor chip and the susceptibility to photolithographic imperfections. Larger single-mode guides can be achieved using an improved epilayer design [95], shown in Fig. 14 for a deeply etched rib guide. Insertion of a layer of low refractive index (less than both the guiding and lower cladding) between guide and lower cladding layers permits single-mode operation for rib widths W as large as 5.5 μm, as compared to <2.5 μm for correspondingly deeply etched conventional structures without the additional layer at $\lambda = 1.5$ μm. Higher-order modes of the conventional structures behave as leaky modes in the improved design, resulting in single-mode behavior. Experiments show that bend performance comparable to conventional guides ($R_1 = 300$ μm) can be achieved for $W < 4$ μm, but some degradation in bend performance ($R_1 = 1.2$ mm) occurs in wider guides.

The increasing bend loss for wider guides reported in [95] is consistent with the onset of modal mismatch loss at straight-to-bent transitions, as is the weak radius dependence of the loss observed for large W, which does not show the strong exponential dependence seen for distributed radiation (e.g., Fig. 7) [36], [46], [67]. Similar radius dependence has been observed in other wide rib guides ($W = 7$ to 16 μm) [13], [56], suggesting that modal mismatch may place significant constraints on wide rib bends; this interpretation is further supported by observed bend near-field intensity distributions [56]. Use of more sophisticated bend patterns, involving lateral offsets at straight-to-bent transitions, may significantly improve such mismatch problems [76]. By employing such offsets as well as width changes in the bend section, low bend junction loss has been achieved at the junction between bends and narrow (1.9 μm) straight guides [76], this approach to low-loss bending offers the additional advantage of directly exciting "whispering gallery modes" [45] of low radiation loss in the bend.

An additional loss mechanism of considerable interest is the coupling loss from semiconductor guides to both on-chip devices (e.g., lasers, detectors) and external optical inputs (e.g., optical fibers). In general, semiconductor waveguides tend to exhibit small mode size perpendicular to the substrate plane because of the large index differences obtained by alloy composition variations. These small mode sizes are well suited for coupling to lasers and detectors; the major difficulty in such coupling is the realization of the required change in material transparency (e.g., transparent guide to absorbing detector), as discussed in Section II-A. Coupling to single-mode optical fibers requires matching to the large fiber mode size (8–10 μm diameter), however, which is more difficult to achieve with single-mode III–V guides. One approach has been to use external, off-chip optical elements (lensed fibers, microlenses, etc.) for mode matching. This technology, developed primarily for laser-fiber coupling, can be directly applied to waveguide coupling problems. Its major disadvantages for small guide mode size are that loss reduction is limited by lens aberrations (typically to several decibels) [96] and submicron alignment tolerances are required [96]. The alternative approach is to create III–V waveguide structures with large mode size, which requires small refractive refractive index changes $\Delta n = 5 \times 10^{-3}$ to maintain single-mode operation. Small Δn is difficult to achieve in a controllable fashion using bulk alloys; reports for the GaAs-AlGaAs system show $\Delta n \geq 10^{-2}$, corresponding to Al mole fraction changes ≥ 0.02 and fiber mismatch loss ≥ 1.5 dB [13], [40], [97]. Smaller index differences can be achieved using carrier concentration changes in n^-/n^+ guides, leading to mismatch loss as low as 1 dB [13], [35], [98], however, such guides exhibit higher propagation loss due to free carrier absorption, and they are often incompatible with high-speed optoelectronic integration due to the conducting substrate.

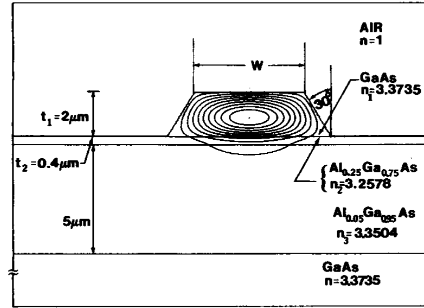

Fig. 14. Waveguide design for large mode size plus compact bend capability [94]. Simulated modal field distribution is shown. The thin $Al_{0.25}Ga_{0.75}As$ depressed-index layer increases confinement under the rib without introducing additional modes.

At present, two solutions to the small Δn problem exist for III–V materials. The first is the antiresonant reflecting guide structure, which does not require accurate Δn control and has demonstrated large mode size [99]. These structures formally support only leaky waveguide modes, and can use a guiding core layer with the same index as the substrate material. In practice, fundamental mode leakage can be significantly reduced (e.g., $\alpha = 0.9$ dB/cm) [100] while maintaining a high leakage for possible higher order modes; thus, effective single-mode operation is achieved. An alternative is the use of diluted multiple quantum wells, material with a large barrier-to-well thickness ratio, in order to controllably achieve small Δn for use in conventional guide structures. This approach has led to InP-based guides with 0.2 dB modal mismatch and 0.8 dB fiber-to-fiber insertion loss for 11 mm long guides butt coupled to single-mode fibers [24], and has been applied to directional couplers with low total insertion loss [101].

B. Electrode Losses in Active Waveguide Devices

The discussion above has focused on the problems of losses in *passive* straight and bent waveguide routing elements. In order to utilize such technology for low-loss *active* III–V components such as switches and modulators, the issue of electrode absorption loss must also be addressed. Optical switching devices employing electronic control signals require a rectifying semiconductor junction based on either doping (p–n junction) or metallization (Schottky contact). Unlike waveguides in other

electrooptic materials (e.g., $LiNbO_3$), it is usually impractical to use thin layers of low index buffer materials (e.g., SiO_2) to minimize optical absorption in metal electrodes. Such layers introduce additional insulator/semiconductor interface states which interfere with proper rectifying operation of the device and can also introduce drift and leakage problems. Thus, most III–V modulators are p-i-n or Schottky devices; the latter primarily restricted to GaAs–AlGaAs devices, whereas p-i-n structures are normally used for InP–InGaAsP due to the low Schottky barrier heights achievable with InP-based materials. Since electrode materials (metal or doped semiconductor) for active modulators must be conducting, modulators exhibit excess propagation loss due to electrode absorption above that obtained in passive waveguides without electrodes. This loss can be minimized by reducing the overlap of the waveguide mode intensity distribution with the doped material (see Section II), but at the expense of modulator efficiency. In devices driven by electric fields (e.g., reversed biased junctions employing electroabsorption [20] or electrooptic effects [68], [102]), increased separation between electrodes to reduce modal overlap also reduces the field achieved for a given applied voltage, and hence the efficiency. In devices driven by injection currents (forward biased junctions), separation of driving electrodes decreases the volume charge density achieved for a fixed injection current, and hence the efficiency. Therefore, a tradeoff exists between electrode loss and modulator efficiency. For fixed drive voltage, this implies a *fundamental tradeoff between the size and loss of waveguide modulators.* The following discussion will focus on how such tradeoff constraints can be minimized for the particular case of reverse-biased junction devices; similar arguments apply to injection modulators.

To quantify loss-efficiency tradeoffs, a figure of merit based on the switching voltage V, device length L, and propagation loss α can be used [102]. Modulator efficiency can be described by the VL product, where V is the voltage required to achieve a large extinction in amplitude modulators or a π phase shift in phase modulators, and L the device length. As modulator efficiency decreases, a longer device is required to maintain a fixed drive voltage and the insertion loss αL increases; thus, an appropriate figure of merit is the αVL product in dB · V, which is the insertion loss (in dB) of a device requiring an applied switching voltage of 1 V. Erman [102] has recently surveyed a variety of electrooptic and electroabsorptive devices and has concluded that, in both cases and for a large number of reported results, the best performance achievable has been $\alpha VL \approx 6$ dB · V. Use of αVL gives a somewhat oversimplified view of the modulator loss problem, because it also includes intrinsic material loss not associated with electrode absorption, and because it does not correctly represent theoretically anticipated tradeoffs between efficiency and loss. Fig. 15 shows theoretical calculations for αVL in GaAs–AlGaAs alloy p-i-n electrooptic phase modulators, indicating that arbitrarily small αVL should be attainable provided that α represents only electrode losses; in practice, however, residual material losses prevent experimental realization of $\alpha VL \approx 0$. Nonetheless, αVL does provide a useful benchmark for evaluating modulator performance.

Modulator losses can be minimized to some extent by the choice of electrode materials. Low doping density should be used in p-i-n devices; however, minimum doping levels are typically limited by depletion effects to the order of $10^{17}/cm^3$ concentration [17], [60]. Similarly, certain Schottky metals introduce less absorption due to differences in the metal dielectric function [103]. In addition, αVL can be improved by using

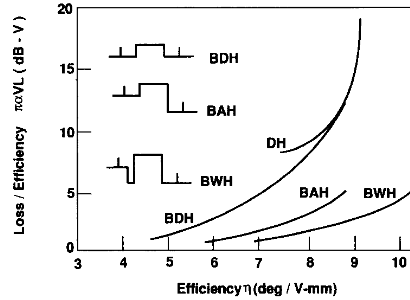

Fig. 15. Low-loss waveguide modulator design, showing calculated electrode loss at fixed 1 V driving voltage αVL versus efficiency for bulk GaAs–AlGaAs electrooptic phase modulators at $\lambda = 1.52$ μm. Curves pertain to the modulator design indicated in the inset, which shows refractive index versus profiles and the location of the p and n electrode materials. Fixed doping $n = p = 2 \times 10^{17}/cm^3$ and 25% n-side Al mole fraction are assumed.

switching phenomena with intrinsically higher efficiency. For example, phase shifters employing depletion-edge translation for charge control [104] have achieved $\alpha VL = 1.2$ dB · V [105]. Similarly, improved αVL may result from the enhanced electroabsorption and electrooptic effects in MQW materials [3].

An alternative method for reducing electrode absorption involves the use of improved epilayer designs to minimize modal overlap with electrodes [68]. Fig. 15 summarizes tradeoffs between αVL and modulator efficiency (phase change per VL), calculated for GaAs–AlGaAs heterostructure modulators utilizing the bulk GaAs electrooptic effect and fixed p-i-n electrode doping of $2 \times 10^{17}/cm^3$. The various curves correspond to single-mode devices utilizing the different refractive index profiles shown in the inset to the figure. Conventional devices utilize a double heterostructure (DH) in which the doping extends to the GaAs–AlGaAs heterointerface, as in [40]. As the GaAs core thickness is decreased, the efficiency can be increased at the expense of increased loss αVL. A similar tradeoff applies to the buffered double heterostructure (BDH), in which a buffer of undoped cladding AlGaAs material is inserted between the doped electrode material and guiding core; this permits realization of single-mode devices with low αVL, at the expense of lower efficiency (whereas unbuffered DH devices would be multimode in this regime). The loss-efficiency tradeoff is improved in a buffered, asymmetric double heterostructure (BAH) with lower index AlGaAs cladding on the p-side of the device. The BAH achieves lower loss αVL at given efficiency because its asymmetry offsets the intrinsically higher p-material absorption (Section II), and because it improves modal overlap with the applied electric field to achieve larger efficiency. Further improvement is obtained using a buffered W heterostructure (BWH), in which a thin depressed-index cladding is inserted between the n electrode and guiding core.

Fig. 16 shows the quantitative refractive index profile and modal intensity distribution for a BWH p-i-n phase modulator based on an $Al_{0.05}Ga_{0.95}As$ n-electrode, GaAs guiding core, and $Al_{0.25}Ga_{0.75}As$ depressed index cladding regions, which employs the bulk GaAs electrooptic effect for switching. The calculated optical intensity shows very little overlap with the doped electrode regions, while only slightly increasing the undoped (i-type) material over which the modulation electric field is applied. The device of Fig. 16 experimentally exhibited $VL = 6$ V · cm, $\alpha = 0.4$ dB/cm (unmetallized), and $\alpha VL = 2.4$ dB ·

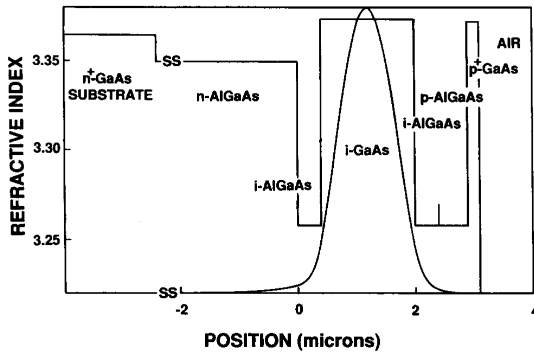

Fig. 16. Low-loss waveguide modulator design, showing refractive index profile and optical intensity distribution (smooth curve) [68].

V [68]. The observed propagation loss is five times smaller than DH devices of comparable efficiency ([40], [102]), demonstrating that proper epilayer design can significantly reduce modulator loss while maintaining high efficiency. Calculations indicate that only ≈ 0.1 dB/cm of the observed α results from electrode absorption, with the additional loss arising from sources intrinsic to the undoped guide. Therefore, proper epilayer design should reduce αVL by fators of ≈ 20 in devices for which electrode losses dominate α. Obvious candidates for loss reduction by such techniques are the electroabsorption modulators currently of interest for high-speed low-chirp applications [20], in which losses are dominated by intervalence band absorption in the p-semiconductor electrode.

V. Discussion

The results discussed in Section IV amply demonstrate that insertion loss alone, including the problem of fiber coupling, is no longer a serious barrier to the use of III–V semiconductor integrated optics. As a result of improvement in epitaxial growth and waveguide channel fabrication techniques, straight guide propagation loss has been reduced to levels comparable to that in $LiNbO_3$ [60], [61], and to the point where overall insertion loss is usually dominated by other factors, such as coupling or additional tradeoffs imposed by application-specific requirements. Devices with low *total* insertion loss, including fiber coupling, comparable to $LiNbO_3$ have also been demonstrated; for example, an InP–InGaAsP 3 dB coupler for coherent receivers with only 1.6 dB insertion loss has been realized [101]. This work has been successfully extended to compact bend and modulator structures with low propagation loss.

The utility of III–V materials for guided-wave device applications depends on other factors besides insertion loss, however, including the relative merits of alternative materials technologies (fiber-, Si-, or insulator-based). Perhaps the greatest advantage of III–V integrated optics lies in monolithic optoelectronic integration, with the major disadvantage continuing to be high material cost/large device size. For integrated devices, there will be tradeoffs between material costs of monolithic integration versus multiple component/assembly costs of hybrid approaches. While the application-specific details of such tradeoffs are beyond the scope of this review, interested readers may find a useful analogy with GaAs monolithic microwave integrated circuits (MMIC's). MMIC's employing GaAs transmission lines exhibit the same "unfavorable device-chip area ratio" [106], [107] as certain III–V guided-wave devices; the relative advantages of MMIC's versus hybrid approaches (employing insulator-based transmission lines) have recently achieved much attention [6], [106], [107].

Therefore, III–V guided-wave device size remains a key issue. Conventional devices with multiple input/output ports are usually limited by bend size as in [72], while finite modulator length (≥ 1 mm for bulk electrooptic directional couplers) [1] limits certain applications. Section IV details tradeoffs between propagation loss and bend or modulator size which critically affect device-chip area limitations. Although device applications may tend toward minimum-size rather than minimum-loss solutions, signal-to-noise constraints on the maximum tolerable loss will ultimately limit device size. As improved modulator switching mechanisms lead to shorter switching structures $\ll 1$ mm [108], [109], bend size will become increasingly important. Despite the significant advances in compact, low-loss bend and mirror structures chronicled above, further work in this area is essential for widespread application of III–V integrated optics. One example is the need for adiabatic transitions from compact bend structures to shallowly etched directional couplers. Recent development of dynamic etch mask techniques [110] could provide such transitions in a compact, low-loss fashion.

In addition to tradeoffs between bend or modulator size and *propagation* loss, there also exist fundamental tradeoffs versus *external coupling* loss. External, off-chip coupling becomes easier for larger mode size, at the expense of increased bend size and modulator efficiency (Section IV). We have already seen that epitaxial III–V guides based on alloy composition changes are best suited for small mode size, which yields the best on-chip performance for bends, modulators, and coupling to lasers and detectors. Since input coupling difficulties associated with small mode size are already encountered in discrete semiconductor laser packaging, monolithic laser/guide integration introduces no additional external coupling difficulty and can thus be quite attractive. In contrast, monolithic integration of small-mode guides with photodetectors increases input coupling difficulty with respect to top-illuminated detectors; similarly, III–V integrated optic modulators and switches typically exhibit greater input/output coupling loss than corresponding $LiNbO_3$ devices. For this reason, III–V waveguide circuits will require low-loss compact transition regions to obtain large guide mode size at the chip edges for ease of external coupling. Several techniques for achieving such transitions have already been demonstrated [96], [111], [112].

VI. Summary

We have reviewed recent progress in the achievement of compact, low-loss waveguide structures using III–V semiconductor materials. Significant advances have resulted in a research shift from work on the general issues of improved material transparency and straight guide propagation loss to more application-specific areas. In particular, size–loss tradeoffs in bend and modulator structures remain key issues for widespread use of III–V integrated optics. We have discussed methods for improving such tradeoffs, and expect continued progress due to the high research interest in these areas.

Acknowledgment

The authors would like to acknowledge many fruitful collaborations, which were essential to obtaining several of the results presented in this paper, with R. Bhat, R. J. Hawkins, A Yi-

Yan, E. Colas, J. P. Harbison, M. Seto, L. M. Schiavone, L. T. Florez, A. Shahar, and C. P. Yun. R. J. Deri also acknowledges fruitful collaborations with O. Wada, M. Makiuchi, N. Yasuoka, A. Kuramata, and S. Yamakoshi of Fujitsu Laboratories. They also wish to thank W. J. Tomlinson for critical reading of the manuscript.

References

[1] E. Garmire, "Semiconductor components for monolithic applications," in *Integrated Optics*, T. Tamir, Ed. New York: Springer-Verlag, 1985, pp. 243-304.

[2] S. Y. Wang, S. H. Lin, and Y. M. Huang, "GaAs travelling-wave polarization electro-optic waveguide modulator with bandwidth in excess of 20 GHz at 1.3 μm," *Appl. Phys. Lett.*, vol. 51, pp. 83-85, 1987.

[3] T. H. Wood, "Multiple quantum well waveguide modulators," *J. Lightwave Technol.*, vol. 6, pp. 743-757, 1988.

[4] A. Podell, S. Moghe, D. Lockie, and F. Ali, "GaAs real estate," *Microwave J.*, pp. 208-212, Nov. 1987.

[5] G. B. Hocker and W. K. Burns, "Mode dispersion in diffused channel waveguides by the effective index method," *Appl. Opt.*, vol. 16, pp. 113-118, 1971.

[6] Y. Bourbin, A. Enard, R. Blondeau, D. Rondi, and M. Papuchon, "Very low loss waveguides and efficient modulators in InGaAsP/InP," in *Integrated and Guided-Wave Optics, 1989 Tech. Dig. Ser.*, vol. 4. Washington, DC: Opt. Soc. Amer., 1989, pp. 110-112.

[7] L. D. Westbrook, P. N. Robson, and A. Majerfeld, "Strain-induced optical waveguiding in GaAs epitaxial layers at 1.15 μm," *Electron. Lett.*, vol. 15, pp. 99-100, 1979.

[8] T. Touam, C. Wu, Y. Gigase, M. Belanger, J. F. Currie, and S. I. Najafi, "Fabrication, characterization, and analysis of zinc-diffused GaAs waveguides," *IEEE J. Quantum Electron.*, vol. 25, pp. 850-853, 1989.

[9] Y. Ohmori, A. Tate, and M. Kobayashi, "GaAs/AlAs multi-quantum-well optical waveguides fabricated by disordering superlattices," *Japan. J. Appl. Phys.*, vol. 26, pp. 1600-1601, 1987.

[10] J. Werner, E. Kapon, N. E. Stoffel, E. Colas, S. A. Schwarz, C. L. Schwarz, and N. Andreadakis, "Integrated external cavity GaAs/AlGaAs lasers using selective quantum well disordering," *Appl. Phys. Lett.*, vol. 55, pp. 540-542, 1989.

[11] U. Koren, T. L. Koch, B. I. Miller, G. Eisenstein, and R. H. Bosworth, "Wavelength division multiplexing light source with integrated quantum well tunable lasers and optical amplifiers," *Appl. Phys. Lett.*, vol. 54, pp. 2056-2058, 1989.

[12] C. J. Chang-Hasnain, E. Kapon, J. P. Harbison, and L. T. Florez, "Integrated external cavity quantum well laser array using single epitaxial growth on a patterned substrate," *Appl. Phys. Lett.*, vol. 56, pp. 429-431, 1990.

[13] H. Inoue, K. Hiruma, K. Ishida, T. Asai, and H. Matsumura, "Low loss GaAs optical waveguides," *J. Lightwave Technol.*, vol. LT-3, pp. 1270-1275, 1985.

[14] E. Kapon and R. Bhat, "Low-loss single-mode GaAs/AlGaAs optical waveguides grown by organometallic vapor phase epitaxy," *Appl. Phys. Lett.*, vol. 50, pp. 1628-1630, 1987.

[15] W. G. Spitzer and J. M. Whelan, "Infrared absorption and electron effective mass in n-type Gallium Arsenide," *Phys. Rev.*, vol. 114, p. 59-63, 1959.

[16] O. K. Kim and W. A. Bonner, "Infrared reflectance and absorption of n-type InP," *J. Electron. Mater.*, vol. 12, pp. 827-836, 1983.

[17] A. A. Ballman, A. M. Glass, R. E. Nahory, and H. Brown, "Double doped low etch pit density InP with reduced optical absorption," *J. Cryst. Growth*, vol. 62, pp. 198-202, 1983.

[18] R. Braunstein and E. O. Kane, "The valence band structure of the III-V compounds," *J. Phys. Chem. Solids*, vol. 23, pp. 1423-1431, 1962.

[19] H. C. Casey, Jr., D. D. Sell, and K. W. Wecht, "Concentration dependence of the absorption coefficient for n- and p-type GaAs between 1.3 and 1.6 eV," *J. Appl. Phys.*, vol. 46, pp. 250-257, 1975.

[20] H. Sano, H. Inoue, Y. Sasaki, H. Nakamura, K. Ishida, and J. M. Glinski, "Low-loss single-mode InGaAs/InAlAs multiquantum well electroabsorption modulator," in *Tech. Dig. Opt. Fiber Commun. Conf.*, San Francisco, CA, Jan. 1990, paper WM 15, p. 112.

[21] C. H. Henry, R. A. Logan, F. R. Merritt, and J. P. Luongo, "The effect of intervalence band absorption on the behavior of InGaAsP lasers," *IEEE J. Quantum Electron.*, vol. QE-19, pp. 947-952, 1983.

[22] G. M. Martin, "Optical assessment of the main electron trap in bulk semi-insulating GaAs," *Appl. Phys. Lett.*, vol. 39, pp. 747-748, 1981.

[23] G. W. Iseler, "Properties of InP doped with Fe, Cr, or Co," in *Proc. 7th Int. Symp. GaAs and Related Compounds*, Inst. Phys. Conf. Ser. No. 45, London, 1978, pp. 144-153.

[24] R. J. Deri, N. Yasuoka, M. Makiuchi, A. Kuramata, and O. Wada, "Efficient fiber coupling to low-loss diluted multiple well optical waveguides," *Appl. Phys. Lett.*, vol. 55, pp. 1495-1497, 1989.

[25] Y. H. Lo, R. J. Deri, J. P. Harbison, B. J. Skromme, M. Seto, M. D. Hwang, and T. P. Lee, "GaAs-on-InP heteroepitaxial waveguides grown by molecular beam epitaxy," *Appl. Phys. Lett.*, vol. 53, pp. 1242-1244, 1988.

[26] E. Garmire, H. Stoll, A. Yariv, and R. G. Hunsperger, "Optical waveguiding in proton-implanted GaAs," *Appl. Phys. Lett.*, vol. 21, pp. 87-88, 1972.

[27] M. Kawabe, N. Kanzaki, K. Masuda, and S. Namba, "Effects of ion etching on the properties of GaAs," *Appl. Opt.*, vol. 17, pp. 2556-2561, 1978.

[28] D. Marcuse, "Mode conversion caused by surface imperfections of a dielectric slab waveguide," *Bell Syst. Tech. J.*, vol. 48, pp. 3187-3215, 1969.

[29] —, "Radiation losses of dielectric waveguides in terms of the power spectrum of the wall distortion function," *Bell Syst. Tech. J.*, vol. 48, pp. 3233-3242, 1969.

[30] G. H. Ames and D. G. Hall, "Attenuation in planar optical waveguides: Comparison of theory and experiment," *IEEE J. Quantum Electron.*, vol. QE-19, pp. 845-853, 1983.

[31] P. K. Tien, "Light waves in thin films and integrated optics," *Appl. Opt.*, vol. 10, pp. 2395-2419, 1971.

[32] M. S. Stern, P. C. Kendall, R. C. Hewson-Browne, P. N. Robson, and D. A. Quinney, "Scattering loss from rough sidewalls in semiconductor rib waveguides," *Electron. Lett.*, vol. 25, pp. 1231-1232, 1989.

[33] F. P. Payne and J. P. R. Lacey, "New analysis of loss in optical waveguides from random wall imperfections," presented at the Topic Meet. Integrated Photon. Res., Hilton Head, SC, Mar. 1990, paper MD5.

[34] R. J. Deri, E. Kapon, and L. M. Schiavone, "Scattering in low-loss GaAs/AlGaAs rib waveguides," *Appl. Phys. Lett.*, vol. 51, pp. 789-791, 1987.

[35] P. Buchmann, H. Kaufmann, H. Melchior, and G. Guekos, "Reactive ion etched GaAs optical waveguide modulators with low loss and high speed," *Electron. Lett.*, vol. 20, pp. 295-296, 1984.

[36] M. W. Austin and P. G. Flavin, "Small-radii curved rib waveguides in GaAs/AlGaAs using electron-beam lithography," *J. Lightwave Technol.*, vol. LT-1, pp. 236-240, 1983.

[37] R. J. Deri, R. J. Hawkins, and E. Kapon, "Rib profile effects on scattering in semiconductor optical waveguides," *Appl. Phys. Lett.*, vol. 53, pp. 1483-1485, 1988.

[38] A. Yi-Yan, R. J. Deri, M. Seto, and R. J. Hawkins, "GaAs/AlGaAs asymmetric Mach-Zehnder demultiplexer with reduced polarization dependence," *IEEE Photon. Technol. Lett.*, vol. 1, pp. 83-86, 1989.

[39] R. G. Walker, H. E. Shepherd, and R. R. Bradley, "Narrow, high-NA GaAs/GaAlAs optical waveguides with losses below 0.7 ± 0.1 dB/cm," *Electron. Lett.*, vol. 23, pp. 362-364, 1987.

[40] S. H. Lin, S. Y. Wang, S. A. Newton, and Y. M. Houng, "Low-loss GaAs/GaAlAs strip-loaded waveguides with high coupling efficiency to single-mode fibers," *Electron. Lett.*, vol. 21, pp. 597-598, 1985.

[41] R. J. Deri, E. Kapon, R. Bhat, and M. Seto, "Low-loss GaInAsP/InP multiple quantum well optical waveguides," *Appl. Phys. Lett.*, vol. 54, pp. 1737-1739, 1989.

[42] E. Garmire, "Optical waveguides in single layers of GaAlAs grown on GaAs substrates," *Appl. Phys. Lett.*, vol. 23, pp. 403-404, 1973.

[43] E. A. H. Marcatili, "Bends in optical dielectric guides," *Bell Syst. Tech. J.*, vol. 48, pp. 2103-2132, 1969.

[44] M. Heiblum and J. H. Harris, "Analysis of curved optical waveguides by conformal transformation," *IEEE J. Quantum Electron.*, vol. QE-11, pp. 75-83, 1975.
[45] S. Sheem and J. R. Whinnery, "Modes of a curved surface waveguide for integrated optics," *Wave Electron.*, vol. 1, pp. 105-116, 1975.
[46] R. J. Deri, E. Kapon, and L. M. Schiavone, "Bend losses in GaAs/AlGaAs optical waveguides," *Electron. Lett.*, vol. 23, pp. 845-847, 1987.
[47] J. S. Gu, P. A. Besse, and H. Melchior, "Novel method for analysis of curved optical rib waveguides," *Electron. Lett.*, vol. 25, pp. 278-280, 1989.
[48] R. J. Deri and R. J. Hawkins, "Polarization, scattering and coherent effects in semiconductor rib waveguide bends," *Opt. Lett.*, vol. 13, pp. 922-924, 1988.
[49] P. C. Kendall, M. S. Stern, and P. N. Robson, "Huygens-type formula for curvature loss from dielectric waveguides in optoelectronics," *Electron. Lett.*, vol. 23, pp. 850-851, 1987.
[50] P. C. Kendall, P. N. Robson, and J. E. Sitch, "Rib waveguide curvature loss: The scalar problem," *IEE Proc.*, vol. 132, pt. J, pp. 140-145, 1985.
[51] C. Rolland, G. Mak, K. E. Fox, D. M. Adams, A. J. Springthorpe, D. Yevick, and B. Hermansson, "Analysis of strongly guiding rib waveguide S-bends: Theory and experiment," *Electron. Lett.*, vol. 25, pp. 1256-1257, 1989.
[52] P. D. Swanson, F. Julien, M. A. Emanuel, L. Sloan, T. Tang, T. A. DeTemple, and J. J. Coleman, "Low-loss semiconductor waveguide bends," *Opt. Lett.*, vol. 13, pp. 245-247, 1988.
[53] L. M. Johnson, Z. L. Liau, and S. H. Groves, "Low-loss GaInAsP buried-heterostructure optical waveguide branches and bends," *Appl. Phys. Lett.*, vol. 44, p. 278-280, 1984.
[54] P. Buchmann and H. Kaufmann, "GaAs single-mode rib waveguides with reactive ion-etched totally reflecting corner mirrors," *J. Lightwave Technol.*, vol. LT-3, pp. 785-788, 1985.
[55] M. J. Robertson, S. Ritchie, and P. Dayan, "Semiconductor waveguides: Analysis of coupling between rib waveguides and optical fibers," in *Proc. SPIE, Integrated Optic. Circuit Eng. II*, vol. 578, S. Siriam, Ed., pp. 184-191, 1985.
[56] R. J. Deri, N. Yasuoka, M. Makiuchi, A. Kuramata, and O. Wada, "Bend performance of fiber-matched optical waveguides on InP," *Electron. Lett.*, vol. 26, pp. 321-322, 1990.
[57] F. K. Reinhart, J. C. Shelton, R. A. Logan, and B. W. Lee, "MOS rib waveguide polarizers," *Appl. Phys. Lett.*, vol. 36, pp. 237-240, 1980.
[58] E. Kapon, N. G. Stoffel, E. A. Dobisz, and R. Bhat, "Birefringence channel waveguide defined by impurity-induced superlattice disordering," *Appl. Phys. Lett.*, vol. 52, pp. 351-353, 1988.
[59] R. J. Deri, N. Yasuoka, M. Makiuchi, A. Kuramata, and O. Wada, "Polarization-dependent modal properties of diluted multiple-quantum-well optical waveguides," *Electron. Lett.*, vol. 25, pp. 1162-1163, 1989.
[60] J. J. Veselka and S. K. Korotky, "Optimization of Ti:$LiNbO_3$ optical waveguides and directional coupler switches for 1.56 μm wavelength," *IEEE J. Quantum Electron.*, vol. QE-22, pp. 933-938, 1986.
[61] P. G. Suchoski and R. V. Ramaswamy, "Minimum-mode-size low-loss Ti:$LiNbO_3$ channel waveguides for efficient modulator operation at 1.3 μm," *IEEE J. Quantum Electron.*, vol. QE-23, pp. 1673-1679, 1987.
[62] R. G. Walker, "Simple and accurate loss measurement technique for semiconductor optical waveguides," *Electron. Lett.*, vol. 21, pp. 581-583, 1985.
[63] R. G. Walker and R. C. Goodfellow, "Attenuation measurements on MOCVD-grown GaAs/GaAlAs optical waveguides," *Electron. Lett.*, vol. 19, pp. 590-592, 1983.
[64] R. Kiel and R. Auracher, "Coupling of single-mode Ti-diffused $LiNbO_3$ waveguides to single-mode fibers," *Opt. Commun.*, vol. 30, pp. 23-28, 1979.
[65] M. W. Austin and P. C. Kemeny, "Measurement of semiconductor optical waveguide loss using a Fabry-Perot interference technique," in *Proc. 3rd Euro. Conf. Integrated Opt.*, H. P. Nolting and R. Ulrich, Eds. New York: Springer, 1985, pp. 140-143.
[66] R. Regener and W. Sohler, "Loss in low finesse Ti:$LiNbO_3$ optical waveguide resonators," *Appl. Phys. B*, vol. 36, pp. 143-147, 1985.
[67] H. Takeuchi and K. Oe, "Low-loss single-mode GaAs/AlGaAs miniature optical waveguides with straight and bending structures," *J. Lightwave Technol.*, vol. 7, pp. 1044-1054, 1989.
[68] R. J. Deri, E. Kapon, J. P. Harbison, M. Seto, C. P. Yun, and L. T. Florez, "Low-loss GaAs/AlGaAs waveguide phase modulator using a W-shaped index profile," *Appl. Phys. Lett.*, vol. 53, pp. 1803-1805, 1988.
[69] T. Ikegami, "Reflectivity of mode at facet and oscillation mode in double-heterostructure injection lasers," *IEEE J. Quantum Electron.*, vol. QE-6, pp. 470-476, 1972.
[70] J. Buus, "Analytical approximation for the reflectivity of DH lasers," *IEEE J. Quantum Electron.*, vol. QE-17, pp. 2256-2257, 1981.
[71] P. W. A. McIlroy, P. M. Rodgers, J. S. Singh, P. C. Spurdens, and I. D. Henning, "Low-loss single-mode InP/InGaAsP waveguides grown by MOVPE," *Electron. Lett.*, vol. 23, pp. 701-703, 1987.
[72] R. J. Deri, A. Yi-Yan, R. J. Hawkins, and M. Seto, "GaAs/AlGaAs integrated optic wavelength demultiplexer," *Opt. Lett.*, vol. 13, pp. 1047-1049, 1988.
[73] A. Shahar, A. Yi-Yan, W. J. Tomlinson, E. Kapon, M. Seto, and R. J. Deri, "Direct loss measurement for optical devices incorporating coupled waveguides," presented at the Top. Conf. Integrated Photon. Res., Hilton Head, SC, Mar. 1990, Paper TuD3.
[74] R. K. Hickernell, D. R. Larson, R. J. Phelan, Jr., and L. E. Larson, "Waveguide loss measurement using photothermal deflection," *Appl. Opt.*, vol. 27, pp. 2636-2638, 1988.
[75] N. Nourshargh, E. M. Stan, N. I. Fox, and S. G. Jones, "Simple technique for measuring attenuation of integrated optical waveguides," *Electron. Lett.*, vol. 21, pp. 818-820, 1985.
[76] H. Van Brug, F. H. Groen, Y. S. Oei, J. W. Pedersen, E. C. M. Pennings, D. K. Doeksen, and J. J. G. M. Van der Tol, "Low-loss straight and curved ridge waveguide in LPE-grown GaInAsP," *Electron. Lett.*, vol. 25, pp. 1330-1332, 1989.
[77] M. K. Hibbs-Brenner and C. T. Sullivan, "Low-loss AlGaAs optical rectangular waveguides at 830 nm," *Appl. Phys. Lett.*, vol. 56, pp. 1529-1531, 1990.
[78] A. Carenco, "Semiconductor waveguides in III-V materials for integrated optics," in *Proc. 4th Euro. Conf. Integrated Opt.* Norwich, U.K.: Page, 1987, pp. 1-6.
[79] A. Carenco, G. Herve-Gruyer, L. Menigaux, A. Mircea, and A. Ougazzaden, "Low-loss 3 cm long InP/GaInAsP rib waveguides," *Proc. 5th Euro. Conf. Integrated Opt.*, Paris, France, Apr. 1989, SPIE vol. 1141, Paper 20.
[80] J. H. Angenent, M. Erman, J. M. Auger, R. Gamonal, and P. J. A. Thijs, "Extremely low loss InP/GaInAsP rib waveguides," *Electron. Lett.*, vol. 25, pp. 628-629, 1989.
[81] Y. S. Kim, S. S. Lee, R. V. Ramaswamy, S. Sakai, Y. C. Kao, and H. Shichijo, "Low-loss AlGaAs/GaAs optical waveguides and phase modulator on Si substrate grown by molecular beam epitaxy," *Appl. Phys. Lett.*, vol. 56, pp. 802-804, 1990.
[82] R. J. Deri, R. Bhat, J. P. Harbison, M. Seto, A. Yi-Yan, L. T. Florez, M. Koza, and Y. H. Lo, "Low-loss GaAs/AlGaAs optical waveguides on InP substrates," *IEEE Photon. Technol. Lett.*, vol. 2, pp. 116-117, 1990.
[83] P. M. Petroff, R. C. Miller, A. C. Gossard, and W. Wiegmann, "Impurity trapping, interface structure, and luminescence of GaAs quantum wells grown by molecular beam epitaxy," *Appl. Phys. Lett.*, vol. 44, pp. 217-219, 1984.
[84] P. Albrecht, W. Doldissen, U. Niggebrugge, H. P. Nolting, and H. Schmid, "Self-aligned waveguide mirrors for optical integration on InGaAsP/InP," in *Tech. Dig. 13th Euro. Conf. Opt. Commun.*, vol. I, Helsinki, Finland, Sept. 1987, pp. 239-242.
[85] J. S. Osinski, C. E. Zah, R. Bhat, R. J. Contolini, E. D. Beebe, T. P. Lee, K. D. Cummings, and L. R. Harriott, "Miniature integrated optical beam-splitter in AlGaAs/GaAs ridge waveguides," *Electron. Lett.*, vol. 23, pp. 1156-1158, 1987.
[86] M. Erman, P. Jarry, R. Gamonal, P. Autier, J.-P. Chane, and P. Frijlink, "Mach-Zehnder modulators and optical switches on III-V semiconductors," *J. Lightwave Technol.*, vol. 6, pp. 837-846, 1988.
[87] K. L. Chen and S. Wang, "Cross-talk products in optical directional couplers," *Appl. Phys. Lett.*, vol. 44, pp. 166-168, 1984.
[88] H. A. Haus and N. A. Whitaker, Jr., "Elimination of cross-talk in optical directional couplers," *Appl. Phys. Lett.*, vol. 46, pp. 1-3, 1985.

[89] M. W. Austin, GaAs/AlGaAs curved rib waveguides," *IEEE J. Quantum Electron.*, vol. QE-18, pp. 795-800, 1982.

[90] H. Takeuchi and K. Oe, "Very low loss GaAs/AlGaAs miniature bending waveguide with curvature radii less than 1 mm," *Appl. Phys. Lett.*, vol. 54, pp. 87-89, 1989.

[91] R. J. Deri, M. Seto, A. Yi-Yan, E. Colas, and R. Bhat, "Diffusion-limited etching for compact, low-loss semiconductor integrated optics," *IEEE Photon. Technol. Lett.*, vol. 1, pp. 46-48, 1989.

[92] M. Seto, A. Shahar, R. J. Deri, W. J. Tomlinson, and A. Yi-Yan, "GaAs/AlGaAs single-mode optical waveguides with low propagation loss and strong optical confinement," *Appl. Phys. Lett.*, vol. 56, pp. 990-992, 1990.

[93] M. Seto, R. J. Deri, A. Yi-Yan, E. Colas, W. J. Tomlinson, R. Bhat, and A. Shahar, "Fabrication of submillimeter-radius optical waveguide bends with anisotropic and isotropic wet chemical etchants," *J. Lightwave Technol.*, vol. 8, pp. 264-270, 1990.

[94] J. Singh, I. Henning, M. Harlow, and S. Cole, "Single-mode low-loss buried optical waveguide bends in GaInAsP/InP fabricated by dry etching," *Electron. Lett.*, vol. 25, pp. 899-900, 1989.

[95] R. J. Deri, A. Shahar, E. Colas, W. J. Tomlinson, R. N. Thurston, A. Yi-Yan, and M. Seto, "Single-mode semiconductor optical waveguides with large dimensions suitable for compact bend applications," *Appl. Phys. Lett.*, vol. 57, pp. 2396-2398, 1990.

[96] T. L. Koch, U. Koren, G. Eisenstein, M. G. Young, M. Oron, C. R. Giles, and B. I. Miller, "Tapered waveguide InGaAs/InGaAsP multiple-quantum-well lasers," *IEEE Photon Technol. Lett.*, vol. 2, pp. 88-90, 1990.

[97] H. Yamagata, Y. Kamata, K. Ueki, H. Miyazawa, M. Okubo, and M. Ogai, "Single-mode GaAs/AlGaAs ridge waveguides with low propagation and coupling loss," in *Tech. Dig. 2nd Optoelectron. Conf.*, Tokyo, Japan, Oct. 1988, pp. 144-145.

[98] H. Kaufmann, P. Buchmann, R. Hirter, H. Melchior, and G. Guekos, "Self-adjusted permanent attachment of fibres to GaAs waveguide components," *Electron. Lett.*, vol. 22, pp. 642-643, 1986.

[99] T. L. Koch, U. Koren, G. D. Boyd, P. J. Corvini, and M. A. Duguay, "Antiresonant reflecting optical waveguides for III-V integrated optics," *Electron. Lett.*, vol. 23, pp. 244-245, 1987.

[100] T. L. Koch, W. T. Tsang, and P. J. Corvini, "Spectral dependence of propagation loss in InP/InGaAsP antiresonant reflecting optical waveguides grown by chemical beam epitaxy," *Appl. Phys. Lett.*, vol. 50, pp. 307-309, 1987.

[101] R. J. Deri, N. Yasuoka, M. Makiuchi, A. Kuramata, O. Wada, and S. Yamakoshi, "Low-loss optical directional coupler on InP," *Electron. Lett.*, vol. 25, pp. 1355-1356, 1989.

[102] E. Erman, "Integrated guided-wave optics on III-V semiconductors," in *Proc. 14th Int. Symp. GaAs Related Compounds*, Inst. Phys. Conf. Ser. No. 91, London, 1988, pp. 33-40.

[103] H. Kawaguchi, "GaAs rib-waveguide directional coupler with Schottky barriers," *Electron. Lett.*, vol. 14, pp. 387-388, 1978.

[104] A. Alping, X. S. Wu, T. R. Hausken, and L. A. Coldren, "Highly efficient waveguide phase modulator for integrated optoelectronics," *Appl. Phys. Lett.*, vol. 48, pp. 1243-1245, 1986.

[105] J. H. Angenent, M. Erman, P. J. A. Thijs, M. Renaud, C. Graver, J. M. Auger, R. Gamonal, and J. A. Cavailles, "Optical switches on InP substrates using carrier depletion with driving voltages as low as 4.5 volt," in *Proc. 15th Europ. Conf. Opt. Commun.*, Gothenburg, Sweden, Sept. 1989, pp. 236-239.

[106] R. A. Pucel, "Design considerations for monolithic microwave circuits," *IEEE Trans. Microwave Theory Tech.*, pt. I, vol. MTT-29, pp. 513-534, 1981.

[107] R. S. Pengelly, "Hybrid vs. monolithic microwave circuits: A matter of cost," in *Monolithic Microwave Integrated Circuits*, R. A. Pucel, Ed. New York: IEEE Press, 1985, pp. 35-60.

[108] K. Ishida, H. Nakamura, H. Matsumura, T. Kadoi, and H. Inoue, "InGaAsP/InP optical switches using carrier induced refractive index change," *Appl. Phys. Lett.*, vol. 50, pp. 141-142, 1987.

[109] J. E. Zucker, I. Bar-Joseph, B. I. Miller, U. Koren, and D. S. Chemla, "Compact directional coupler switches using quantum well electrorefraction," *Appl. Phys. Lett.*, vol. 54, pp. 10-12, 1989.

[110] A. Shahar, W. J. Tomlinson, M. Seto, A. Yi-Yan, and R. J. Deri, "Dynamic etch mask technique for fabricating tapered semiconductor optical waveguides and other structures," *Appl. Phys. Lett.*, vol. 56, pp. 1098-1100, 1990.

[111] M. W. Austin, "Fabrication of tapered couplers in GaAs/GaAlAs rib waveguides," *Electron. Lett.*, vol. 24, pp. 284-285, 1988.

[112] D. E. Bossi, W. D. Goodhue, and R. H. Rediker, "Reduced confinement GaAlAs tapered waveguide antenna," in *Tech. Dig. Integrated Guided-Wave Opt.*, Opt. Soc. Amer. Tech. Dig. Ser. vol. 4, Washington, DC, 1989, pp. 80-83.

[113] A. J. N. Houghton, D. A. Andrews, G. J. Davies, and S. Ritchie, "Low-loss optical waveguides in MBE-grown GaAs/AlGaAs heterostructures," *Opt. Commun.*, vol. 46, pp. 164-166, 1983.

[114] U. Das, P. R. Berger, and P. K. Battacharya, "InGaAs/GaAs multiquantum-well electroabsorption modulator with integrated waveguide," *Opt. Lett.*, vol. 12, pp. 820-823, 1987.

[115] M. Erman, N. Vodjdani, J. B. Theeten, and J. P. Cabarnie, "Low loss waveguides grown on GaAs using localized vapor phase epitaxy," *Appl. Phys. Lett.*, vol. 43, pp. 894-895, 1983.

[116] C. H. Joyner, A. G. Dentai, R. C. Alferness, L. L. Buhl, M. D. Divino, and W. C. Dautremont-Smith, "InGaP/InP waveguides," *Appl. Phys. Lett.*, vol. 50, pp. 1509-1511, 1987.

[117] S. Ritchie, E. G. Scott, and P. M. Rodgers, "Optical waveguides in InAlAs grown on InP by MBE," *Electron. Lett.*, vol. 22, pp. 1066-1068, 1986.

[118] J. Pamulapati and P. K. Battacharya, "Single mode optical waveguides and phase shifters using InGaAlAs on InP grown by molecular beam epitaxy," *Appl. Phys. Lett.*, vol. 56, pp. 103-104, 1990.

[119] P. Cinguino, F. Genova, S. Morasca, C. Rigo, and A. Stano, "Low-loss ridge optical waveguides in quaternary InGaAlAs/InP grown by MBE," *Electron. Lett.*, vol. 23, pp. 235-236, 1987.

Robert J. Deri (M'87), photograph and biography not available at the time of publication.

Eli Kapon (M'89–SM'89), photograph and biography not available at the time of publication.